Sleep-Modulated Cross-Frequency Coupling Between δ Phase and β–γ Bistability: A System-Level Modulation of Epileptic Activity

Running head: Coupling Between δ phase and β–γ Bistability

Gaia Burlando[1] MSc, Chiara Belforte[1] MSc, Felix Siebenhühner[2,5] PhD, Luca Di Tullio[3,4], Lorenzo Chiarella[3,4], Vladislav Myrov[5] PhD, Frédéric Zubler[6,7] MD & PhD, Monica Roascio[1] PhD, Francesco Cardinale[8], Satu Palva[2,9] PhD, J Matias Palva[2,5,9] PhD, Lino Nobili[3,4*] MD & PhD, Gabriele Arnulfo[1,4*] PhD, Sheng H Wang[2,5,10–12*] PhD

1. Department of Informatics, Bioengineering, Robotics and Systems Engineering, University of Genoa, Genoa, Italy.
2. Neuroscience Center, Helsinki Institute of Life Science (HiLIFE), University of Helsinki, Helsinki, Finland.
3. Department of Neurosciences, Rehabilitation, Ophthalmology, Genetics and Maternal and Children's Sciences, University of Genoa, Genoa, Italy.
4. Child Neuropsychiatry Unit, IRCCS Istituto Giannina Gaslini, Full Member of the ERN EpiCARE, Genoa, Italy.
5. Department of Neuroscience and Biomedical Engineering, Aalto University, Espoo, Finland.
6. Department of Neurology, Sleep-Wake-Epilepsy Center, Inselspital, Bern University Hospital, University of Bern, Bern, Switzerland.
7. Department of Neurology, Spitalzentrum Biel, University of Bern, Biel, Switzerland.
8. Centre of Epilepsy Surgery "C. Munari", Department of Neuroscience, Niguarda Hospital, Milan, Italy.
9. Centre for Cognitive Neuroimaging, School of Psychology and Neuroscience, University of Glasgow, Glasgow, United Kingdom.
10. CEA, NeuroSpin, Université Paris-Saclay, Gif-sur-Yvette, France.
11. MIND team, Inria, Palaiseau, France.
12. Jack H. Miller Magnetoencephalography Center, Helen DeVos Children's Hospital, Grand Rapids, Michigan, USA.

*Corresponding Author:
lino.nobili@unige.it
sheng.1.wang@aalto.fi

Number of characters in the title (125), the running head (44)
Number of words in Abstract (257), Introduction (480), Discussion (1178), Body of the manuscript (4834 – Introduction + Methods + Results + Discussion)
Number of figures: (5), color figures: (5), and tables (2)

Abstract

Objective: To investigate the mechanistic link between large-scale δ-band (0.5–4 Hz) synchrony during sleep and local bistability of the β–γ band (15–200 Hz), a biomarker of the epileptogenic zone.

Methods: 7–9-hour stereo-EEG sleep recordings were obtained from 14 subjects (22.3 ± 10.8 years old; 7 males) with sleep-related hypermotor epilepsy. These recordings were segmented into 10-minute epochs of uninterrupted interictal N2 and N3 stages of NREM sleep. We assessed phase synchrony, phase-amplitude coupling (PAC), and β–γ band (15–200 Hz) bistability. Canonical correlation analysis was used to explore whether PAC links δ-synchrony to β–γ band bistability.

Results: Compared to non-epileptogenic regions (nEZ), the epileptogenic zone (EZ) exhibited stronger 15–200 Hz bistability and greater 2–8 Hz and 15–100 Hz phase synchrony. Compared to N3, N2 showed stronger PAC between 2–30 Hz phases in nEZ and 5–150 Hz amplitudes in EZ. Canonical correlations between direction-specific δ-modulated PAC and both bistability and synchrony were identified during N2 (r = 0.86 and 0.82) and N3 (r = 0.84 and 0.80), with the strongest contributors being 2–4 Hz synchrony and bistability in 2–4 Hz and 15–200 Hz bands. Correlations between interictal spikes and canonical covariates of bistability and PAC (r^2=0.62 for N2 and 0.56 for N3) validated their relevance to epileptogenicity.

Interpretation: δ-band synchrony and β–γ band bistability play a pivotal role in epileptogenic mechanisms, likely through the coupling of δ phases and β–γ amplitudes across large-scale networks—with a significant contribution from the nEZ tissues.

Abbreviations

CCA: canonical correlation analysis
EZ: epileptogenic zone
FCD: focal cortical dysplasia
PAC: phase-amplitude coupling
RDP: relative δ power, an assessment of δ amplitude instability

Introduction

It is well established that NREM sleep promotes interictal epileptiform discharges (IEDs) and facilitates seizure activity, whereas REM sleep exerts a suppressive effect[1–3]. Experimental and clinical studies have demonstrated that thalamo-cortical and cortical sleep oscillations, which drive the spontaneous emergence of slow waves, spindles, and ripples during NREM sleep, can promote paroxysmal epileptic activity[4–8]. Slow waves exhibit an alternation between “up” and “down” states, with up states linked to the generation of spindles and ripples[9–13]. The transition from the down state to the up state—a period of high neuronal synchronization—has been identified as a key driver of interictal epileptic activity during NREM sleep[14]. Moreover, several studies have shown that IEDs and seizures are more likely to occur during unstable sleep—particularly in N2—where arousal fluctuations depicted by bursts of EEG slow waves (known as the cyclic alternating pattern) are prevalent[15–20]. In contrast, IEDs and seizures occur less frequently during stable sleep (N3), when slow-wave activity peaks. These findings challenge the traditional view that slow waves directly promote epileptic activity. Instead, they suggest that slow waves with prominent waxing-and-waning dynamics—a hallmark of bistable systems[21,22]—may play a pivotal role in epileptogenicity.

Bistability, abrupt switching between two states in activity, represents a large-scale phenomenon observed in the brain and across various complex systems—often preceding sudden onset of catastrophic events such as seizures[21–24] (Fig. 1A). The epileptogenic zone (EZ) exhibits increased β–γ band (15–200 Hz) bistability during resting-state[21,22] and increased bursts of high amplitude β–γ activity during NREM compared to wakefulness[25]. Meanwhile, the EZ is also characterized by aberrant criticality features including strong long-range temporal correlations[26], heightened functional inhibition[22,27], elevated large-scale phase synchrony[22,28,29], and cross-frequency phase-amplitude coupling (PAC)[30,31]. Collectively, these observations reflect maladaptive hyperexcitability[28] and hypersynchrony[30], a deviation from a healthy regime of critical phase transitions between asynchrony and synchrony—a natural attractor for adaptive brain dynamics[32–34]. Nonetheless, it has remained

unclear how unstable dynamics of slow waves, in particular δ-band (0.5–4 Hz), are linked to β–γ band bistability (Fig. 1B).

To better understand how sleep may facilitate epileptic activity, we studied a well-curated cohort of fourteen Sleep Hypermotor Epilepsy (SHE) patients with type 2 Focal Cortical Dysplasia (FCD) (Fig. 1C). These patients underwent overnight SEEG recordings, with MRI-confirmed electrode placement within the FCD tissues. This cohort was chosen because it represents a prototypical clinical model of sleep-related epilepsy with a well-characterized histopathological substrate that significantly increases the risk of seizures during sleep[7,35]. Specifically, we investigated the coupling between waxing-and-waning δ-oscillations—reflecting the characteristic bistable dynamics of the δ-band during unstable sleep[19] (Fig. 1D–E)—and β-γ amplitude dynamics, focusing on amplitude bistability. We hypothesized that the bistable dynamics of large-scale δ-band oscillations during NREM sleep orchestrate epileptic activity within and beyond the EZ, with this effect being most prominent during N2, the most unstable NREM sub-stage.

Methods

Patients and data acquisition

Patients with drug-resistant, Sleep Hypermotor Epilepsy who underwent stereo-EEG recording between July 2011 and December 2015 in the “Claudio Munari” Center for Epilepsy Surgery (Milan, Italy) were retrospectively screened for this study. The selection criteria were as follows: 1) presence of type 2 FCD lesion confirmed by postsurgical histopathological analysis; 2) Presence of recordings from scalp EEG electrodes, electrooculogram, and submental electromyography electrodes; 3) At least one contact located within or at the immediate border of the FCD, identified based on neuroradiological findings and/or a typical intracerebral EEG pattern; 4) Presence of interictal spikes both within and outside the seizure onset zone[36]; and 5) Complete seizure freedom with a minimum of one year of post-surgical follow-up (Engel class 1A[37]), confirming the localization and complete resection of the EZ.

We analyzed data from fourteen subjects who met these criteria (mean age: 22.2 ± 10.8 years, 7 male). SEEG were recorded using Microdeep electrodes D08 (Dixi Medical) or Depth Electrodes Range 2069 (Alcis, France), comprising 5–18 contacts spaced 1.5 mm apart. EEG signals were acquired using a Neurofax EEG-1100 system (Nihon Kohden, Tokyo, Japan) with 1 kHz sampling and 16-bit resolution. Only contacts placed in the cortex were considered. This study was conducted in accordance with the recommendations of the Ethics Commission of Ospedale Niguarda (ID:939). All patients provided written informed consent for the retrospective analysis of their data, in compliance with the Declaration of Helsinki.

Clinical identification of the epileptogenic zone (EZ)

The EZ is the minimum amount of cortex that must be resected, inactivated, or completely disconnected to maintain seizure freedom[38]. In this study, the EZ was identified by expert epileptologists as the seizure onset zone through concordance with electro-anatomic-clinical observations, later confirmed by surgical outcome and histology after seizure resection. Histopathology in all patients confirmed cortical malformations with balloon cells, consistent with type IIb FCD.

SEEG preprocessing

In these fourteen subjects, 487 out of 1626 contacts (29.45 ± 7.90% per subject) were excluded from analysis due to their location in the white matter or the presence of significant artifacts. Line noise at 50 Hz and its harmonics were removed using a filter bank of notch filters with 1 Hz band-stop width. We employed a bipolar referencing scheme by pairing neighboring electrode contacts and excluding a common reference. Bipolar-referenced contacts were categorized based on clinically identified FCD: channels with both contacts entirely within the dysplasia were designated as EZ channels (N=93), while those with both contacts entirely within healthy tissue were classified as nEZ channels (N=1046). Channels that did not meet these criteria were excluded (Tab. 2).

Obtaining interictal N2 and N3 epochs

The SleepSEEG Matlab toolbox was used to identify 10-minute N2 and N3 sleep epochs from 7–9 hours of uninterrupted recordings[39]. Before further analysis, these SEEG epochs were reviewed and validated by physicians in conjunction with the concurrent EOG and EMG. Epochs containing seizure activities were excluded to ensure that only uninterrupted sleep stages were analyzed. A total of 134 and 56 epochs were obtained for N2 and N3, respectively.

Spike detection

Spikes are characterized by high-amplitude, fast activity with widespread spatial diffusion in SEEG recordings, which, if left untreated, would inflate synchrony, bistability, and PAC assessments. We identified the time windows containing spikes following the approach used in our previous study[30]. These windows were defined as 500 ms non-overlapping intervals during which at least 10% of cortical contacts exhibited abnormal sharp peaks—amplitude envelope peaks exceeding five times the standard deviation of the contact mean amplitude—in more than half of the 50 frequency bands (from 2 to 450 Hz). On average, 12.08 ± 12.50 such windows were excluded from the assessments.

Assessing features of neuronal oscillations

We applied a narrow-band Morlet wavelet transform to the SEEG epochs to obtain time-frequency representations[40] using Morlet wavelets with 40 logarithmically spaced center frequencies ranging from 2 to 250 Hz (m=7.5). We followed our previous approach for assessing the δ-instability[19]. Each 10-minute epoch was divided into non-overlapping 5-second windows, yielding 120 windows. The δ-band power was defined as the average Morlet envelope between 0.5 and 4 Hz, and relative delta power (RDP) was calculated by dividing δ-power by the total power across the 0.5–180 Hz spectrum. Spatial instability was defined as the standard deviation across channels after averaging RDP over time bins, and temporal instability as the standard deviation across time bins after averaging RDP across channels.

Neuronal bistability refers to the erratic switching between an up and a down mode in a neuronal oscillation, likely caused by an underlying first-order (discontinuous) phase transition due to strong positive feedback[21,41]. The bistability index (BiS) is estimated by first fitting the sample probability distribution of the narrow-band power time series to a single-exponential (Eq. 1) and a bi-exponential model (Eq. 2), then comparing the fitting using the Bayesian information criterion (BIC). The single-exponential model is defined as:

$$P_{R^2}(R^2) = \gamma e^{-\gamma R^2} \quad (1)$$

where γ is the exponent, and the bi-exponential model is defined as:

$$P_{R^2}(R^2) = \frac{1}{(\delta_1 + \delta_2)}(\delta_1 \gamma_1 e^{-\gamma_1 R^2} + \delta_2 \gamma_2 e^{-\gamma_2 R^2}) \quad (2)$$

where γ_1 , γ_2 are the two exponents and δ_1, δ_2 are weighting factors. The BIC was computed for the single- and bi-exponential fitting as follows:

$$BIC = k \cdot ln\,(n) - 2\,ln\,(\hat{L}) \quad (3)$$

where *n* is the number of samples, $\hat{L}$ is the likelihood function, *k* is the number of free parameters in the model: $k = 1$ for single-exponential BIC_{Exp} and $k = 4$ for bi-exponential model BIC_{biE} . A better-fitted model yields a small BIC value. The difference in BIC between single- and bi-exponential is obtained as:

$$dBIC = BIC_{Exp} - BIC_{biE} \quad (4)$$

and the bistability index BiS as:

$$BiS = \log_{10}(dBIC) \quad \text{if } dBIC > 0 \quad (5)$$

$$BiS = 0 \quad \text{if } dBIC \leq 0$$

A BiS close to zero indicates that the single-exponential model best fits the time series, while a BiS > 3 offers strong support for the bi-exponential model.

Assessing interareal phase synchrony

Synchrony between all bipolar-referenced SEEG electrode contacts was estimated using the phase-locking value (PLV)[42] for the 40 narrow-band frequencies that are evenly spaced on a log10 scale. Considering $x'(t)$ as the narrow-band complex wavelet coefficients of broad-band signal $x(t)$ of a contact, the complex-valued PLV (cPLV) is:

$$cPLV = \frac{1}{T}\sum_{t=1}^{T} \frac{x\prime(t)}{|x\prime(t)|} \cdot \frac{y\prime*(t)}{|y\prime(t)|} \quad (6)$$

where T represents the total sample number, and * is the complex conjugate. The PLV is the absolute value of the cPLV.

To minimize bias and prevent artificially inflated synchrony estimates, we removed entries from the PLV matrices where bipolar channels shared a common contact. Each PLV matrix was treated as a graph, with contacts as nodes and pairwise synchrony as edges. To estimate first-order synchrony derivatives, we used eigenvector centrality (EVC), a measure where a node's centrality is higher if it is connected to other nodes with high centrality. Second-order synchrony derivatives were evaluated using the clustering coefficient (CC), which quantifies the proportion of a node's neighbors that are also interconnected with each other.

Assessing phase-amplitude coupling (PAC)

PAC refers to the modulation of fast neuronal oscillation amplitudes by the phase of slower oscillations in the brain (Fig. 1F) and was assessed using PLV[43]:

$$PLV_{PAC,a,b} = \frac{1}{N}\left|\sum_{n=1}^{N} e^{i\cdot(\theta_{a,LF}-\theta_{b,HF,LF})}\right| \quad (7)$$

where $\theta_{b,HF,LF}$ is the phase of the amplitude envelope of the high-frequency (HF) signal filtered with a Morlet filter at the low frequency (LF). To compute the PAC, we used a design matrix comprising ten LFs, ranging from 1.2 to 68.1 Hz, and 19 slow-to-fast frequency ratios, ranging from 1:2 to 1:100. Having thus computed PAC matrices in a low-frequency-to-ratio format, we projected them to a low-frequency-to-

high-frequency space for enhanced readability and interpolated missing values. Results show normalized PAC (nPAC), where nPAC = $PLV_{PAC,observed}/PLV_{PAC,surrogate}$ (see subsection "statistical analyses" for surrogate creation), so that nPAC > 1 indicates PAC above the null hypothesis level.

Canonical correlation analysis (CCA)

Canonical correlation analysis (CCA) is a statistical procedure that identifies the maximal correlations between two datasets[44] and has been previously used for analyzing high-dimensional neuroscience data[45]. It aims to find canonical weight vectors u and v that maximize the correlations between projected data:

$$\max_{u,v} \rho = \frac{u^T \Sigma_{AB} v}{\sqrt{u^T \Sigma_{AA} u}\sqrt{v^T \Sigma_{BB} v}} \quad (8)$$

where $\Sigma_{AA} = (A^T A)/n$ is the covariance matrix for the data array A (*e.g.*, inward-PAC, size $n \times a$, n is contact number) and $\Sigma_{BB} = (B^T B)/n$ is the covariance matrix for data array B (*e.g.*, bistability, size $n \times b$). $\Sigma_{AB} = (A^T B)/n$ is the cross-covariance of A and B. Solving the generalized eigenvalue problem:

$$\begin{bmatrix} 0 & \Sigma_{AB} \\ \Sigma_{BA} & 0 \end{bmatrix} \begin{bmatrix} u \\ v \end{bmatrix} = \rho \begin{bmatrix} \Sigma_{AA} & 0 \\ 0 & \Sigma_{BB} \end{bmatrix} \begin{bmatrix} u \\ v \end{bmatrix} \quad (9)$$

yields the canonical correlation coefficients ρ and the weight vectors u and v. The canonical variates (CV) are computed as:

$$Z_A = Au \text{ and } Z_B = Bv \quad (10)$$

where Z_A and Z_B (both with size $n \times 1$) are the CVs of A and B; u $(a \times 1)$ and v $(b \times 1)$ are the first canonical weight vectors.

We used CCA to explore the relationships between outward-PAC (how the amplitudes of fast activity in one region are modulated by the phases of slower waves in all other regions) and phase synchrony, as well as inward-PAC (how the phases of slow waves in one region modulate the amplitudes of faster activity in all other regions) and bistability, aiming to uncover potential mechanistic links between large-scale

synchrony and local bistability (Fig. 1G). We focused exclusively on the δ-phase portion of the full PAC design matrix (Fig. 5A, top left; see Fig. 4 for examples of the full PAC design matrix, *i.e.*, all frequency combinations for which PAC was estimated). As each subject had a different number of N2 and N3 epochs, individual PAC connectivity matrices (*e.g.*, 1→80 Hz) were first averaged within subjects so that one PAC matrix represents the mean coupling between a δ-frequency (1 Hz, Fig. 5A, left) and the amplitude of a faster frequency (80 Hz corresponding to 'ratio of 80' for 1 Hz) for a N2 or N3 epoch.

Inward- and outward-PAC vectors were obtained by averaging each PAC connectivity matrix column-wise and row-wise, respectively. Note that 'inward' and 'outward' here refer to the topological structure of the PAC graphs, rather than implying directionality or a causal relationship between the slow and fast modes. The elements in the inward vector represent how a contact's amplitude is influenced by the δ phase of all other contacts, while the elements in the outward vector indicate how the δ phase of one contact modulates the amplitudes of all other contacts (Fig. 5A, bottom left). Pooling the individual inward and outward PAC vectors resulted in corresponding two-dimensional feature arrays, which were then subjected to CCA analysis (Fig. 5A, right). The EVC was used for within-frequency synchrony data as it demonstrates stronger differentiation power for the EZ (Fig. 3).

CVs are linear combinations of variables from each feature dataset that maximize the correlation between the two datasets. We averaged the CVs of contacts' PAC, bistability, and synchrony estimates (*i.e.*, data in Fig. 5D–E) within subjects and found correlations between these coarse-grained neuronal features and number of spikes observed in the same N2 and N3 epochs. Data from fourteen subjects, comprising 1139 SEEG contacts, were pooled for this analysis. The CCA was carried out using the Python *scikit-learn* module[46].

Statistical Analyses

We calculated null-hypothesis distributions for both PLV and PAC using surrogate data. For each contact pair, we split each narrow-band time series into two segments at a random time point, denoted as k. This resulted in two time series:

$$x'_1(t) = x'(1 \ldots k) \text{ and } x'_2(t) = x'(k \ldots T) \quad (11)$$

We then created the surrogate time series, $x'_{surr}(t)$, by concatenating these two segments in reverse order: $x'_{surr}(t) = [x'_2, x'_1]$. The surrogate PLV and PAC were computed across all pairs of channels.

Wilcoxon rank-sum test was used to make comparisons between groups. For PAC, the test was applied to each LF–HF pair over epochs into which the signal was segmented. For amplitude, BiS, EVC, and CC the test was applied to each frequency across the pooled channels. Benjamini-Hochberg (BH) procedure was used to correct for multiple comparisons[47], with the post-correction significance threshold set for $p < 0.05$. Effect size for between-group difference was evaluated with Cohen's *d*, and its confidence intervals under null-hypothesis were measured by label-shuffled surrogates (N=10'000).

Results

N2 shows greater δ-band instability than N3

We compared δ-band instability between N2 and N3 using the Wilcoxon rank-sum test ($\alpha = 0.05$), considering both spatial instability (across contacts) and temporal instability (across time for a contact). When treating each 10-minute run as an independent observation (134 runs for N2, 56 runs for N3), we found that N2 compared to N3 shows significantly higher spatial ($p < 6.5 \times 10^{-9}$) and temporal instability ($p < 8.8 \times 10^{-10}$) (left, Fig. 1E). However, when averaging δ-band instability within subjects, only temporal instability remained significantly higher in N2 compared to N3 ($p < 0.013$), while spatial instability did not reach statistical significance ($p > 0.054$) (right, Fig. 1E).

The EZ is characterized by strong δ band amplitudes and β–γ band bistability

We next examined whether N2 and N3 sleep can be differentiated by amplitudes and bistability across narrow-band oscillations. During slow-wave N3 sleep, the nEZ

showed stronger 2–10 Hz amplitudes than EZ. Compared to N3 sleep, both the EZ and nEZ exhibited greater amplitudes in 10–200 Hz during N2 (Fig. 2B; $p < 0.05$, Wilcoxon rank sum test, multiple comparison corrected with BH procedure). The effect size of these differences (Fig. 2B, bottom) ranged from small to moderate (corresponding to Cohen's $d = 0.2$ and 0.5, respectively).

The EZ and nEZ exhibited different bistability spectra. Compared to N3, the EZ showed smaller 5–45 Hz bistability but larger 130–225 Hz bistability during N2 (Fig. 2C). Conversely, the nEZ showed larger 2–13 Hz bistability and smaller 20–100Hz bistability during N2, with effect size ranging from small to moderate (Fig. 2C, bottom). Moreover, compared to nEZ, the EZ exhibited stronger amplitudes across slow and fast oscillations in both N2 and N3, with a large effect size (Cohen's $d > 0.8$) in 2–30 Hz oscillations during N2 (Fig. 2D). During N2, the nEZ showed stronger 2–7 Hz bistability. EZ showed stronger bistability of high-gamma oscillations, with largest effects in 15–150 Hz during N2 and 6–40 Hz during N3 (Fig. 2E). In summary, the nEZ demonstrated lower amplitudes but larger bistability in δ-oscillations during N2, while the EZ showed lower δ-bistability (*i.e.*, more stable than nEZ) but increased β–γ bistability in N2.

Strong δ and β–γ band synchrony characterizes the EZ

We examined if large-scale phase synchrony differentiates N2 from N3 sleep and the EZ from nEZ contacts. Both eigenvector centrality (EVC) and the clustering coefficient (CC) of the synchrony networks showed weak differentiation between N2 and N3 (Fig. 3A–B). However, both the EZ and nEZ exhibited stronger 2–5 Hz CC during N2 compared to N3 (Fig. 3B, bottom).

During both N2 and N3, the EZ consistently displayed stronger EVC in 2–5 Hz (Cohen's $d > 0.5$) and 20–40 Hz (Cohen's $d > 0.8$) synchrony, while the nEZ showed stronger EVC in 100–300 Hz synchrony, particularly during N2 (Fig. 3C). Additionally, the EZ exhibited stronger CC in the 2–5 Hz range in both N2 and N3 (Fig. 3D).

Together, these findings suggest that elevated δ and β–γ band synchrony characterize the connectivity of the EZ (characterized by EVC) and its neighboring regions (characterized by CC), with a stronger effect during N2 sleep.

Large-scale δ–β band phase coupled with EZ's β–γ band amplitudes (PAC) during N2

The EZ exhibits large β–γ band bistability (Fig. 2) and elevated δ and β–γ band synchrony (Fig. 3), and a potential system-level mechanistic link between these bands was next investigated using PAC analysis. We expected that β–γ amplitudes would be modulated by the δ phase, similar to what has been observed in focal epilepsy in both sleep[48] and resting-state[30].

Across four quadrants of the cohort pooled PAC matrices (Fig 1.F), we observed spectrally widespread connectivity in both N2 and N3 (Fig. 4A–B). In N3, the nEZ→nEZ quadrant demonstrated stronger PAC strength ($p < 0.05$, BH corrected) compared to N2 with large effect size (Cohen's $|d| > 0.8$), particularly between the slowest δ-oscillation (< 1Hz) and β–γ amplitudes (Fig. 4C). Conversely, the EZ→EZ quadrant showed greater PAC strength during N2, most pronounced between the 15–24Hz phase and the amplitudes of fast rhythms (Cohen's $|d| > 0.65$). The EZ→nEZ quadrant showed greater PAC in N2 between β-phase and high-γ amplitudes with a small effect (Cohen's $|d| > 0.25$). Most notably, in N2, the nEZ→EZ quadrant showed stronger PAC between 1–2 Hz phase and widespread fast oscillations, indicating the modulation of γ and high-γ amplitudes in the EZ by δ phase from the nEZ (Fig 4 C, right).

PAC modulated by δ phase is correlated with epileptogenic bistability and synchrony

If PAC serves as a mechanistic link between large-scale δ phase and pathological β–γ band local bistability, it should correlate with both phase synchrony and bistability in a direction-specific manner within PAC connectivity (Fig. 5A). Specifically, inward δ-band PAC—a vector whose elements characterize how the amplitudes of fast

oscillations in one region are modulated by δ phases in other regions—should correlate with bistability, with the strongest effects observed in the β–γ band. Conversely, outward PAC—a vector whose elements characterize how δ phases in one region modulate the amplitudes of fast oscillations in other regions—should correlate with phase synchrony, with the strongest effects observed in the δ-synchrony.

Canonical correlation analysis (Eq. 8–9) revealed that, for both N2 and N3, a strong effect size of correlations (r^2 > 0.6) between inward-PAC and bistability, as well as outward-PAC and synchrony (Fig. 5B–C). The strongest correlation between inward-PAC and bistability was 0.86 for N2 and 0.84 for N3 (Fig. 5D, top row), primarily driven by 2–7 Hz and 20–100 Hz bistability, along with 20–250 Hz amplitudes of inward-PAC (Fig. 5D, bottom row), with a stronger involvement of δ-oscillations during N2. Similarly, the highest correlation between synchrony and outward-PAC was 0.82 for N2 and 0.80 for N3 (Fig. 5E, top row), mainly influenced by 2–5 Hz synchrony and 7–300 Hz outward-PAC (Fig. 5E, bottom row). These findings support our hypothesis that PAC acts as a mechanistic link between δ-synchrony and β–γ bistability.

Correlation of canonical neuronal features with interictal spikes

Lastly, we examined the functional relevance of the canonical correlation between PAC, bistability, and synchrony by analyzing their canonical variates (CVs)—linear combinations of narrow-band estimates (Eq. 10)—in relation to interictal spikes. If δ phase and β–γ amplitude bistability are indeed coupled via a PAC mechanism, their corresponding CVs should be correlated with the spikes, a well-established clinical biomarker of epileptogenicity.

We averaged the CV of contacts' PAC, bistability, and synchrony estimates (*i.e.*, samples in Fig. 5D–E) within subjects and found correlations between these coarse-grained features and the number of spatial bursts of spikes observed from the same N2 and N3 epochs. The correlations between spikes and the CV of inward-PAC and bistability were strong (r^2=0.62 for N2 and 0.56 for N3), while that between outward-PAC and synchrony were weak (r^2=0.22 for N2 and 0.1 for N3). Note that canonical weights were assigned for maximizing correlations (Eq. 9), making the sign of the

correlations irrelevant. These findings validate the functional relevance of the canonical correlations.

Discussion

In this study, we confirm our hypothesis that synchronous but bistable δ oscillations are required to orchestrate dynamics of higher-frequency activity within and outside the EZ. This effect is hence more prominent in N2 when sleep dynamics are more unstable.

Our findings indicate that in the nEZ, δ oscillations were more prominent during N3 sleep but exhibited greater bistability in N2. Additionally, during N3, slow-wave oscillations (≤1 Hz) modulated δ–θ and high-γ amplitudes. In contrast, the EZ showed significantly higher β-γ band bistability and stronger δ-band synchrony compared to nEZ regions, more prominent during N2. Of note, the nEZ δ phase (2–4 Hz) strongly modulates β-γ amplitude of the EZ, particularly during N2 sleep.

β-γ bistability, a hallmark of EZ[22], was strongly correlated with inward-PAC (*i.e.*, β–γ amplitudes driven by δ phase), while δ-phase synchrony correlated with outward-PAC (*i.e.*, δ phase modulating θ and β-γ amplitudes) during NREM sleep, stronger during N2. These converging results suggest that δ-band synchrony networks and local β-γ bistability are interconnected systems-level neuronal mechanisms, mediated by coupling between δ phase and β-γ amplitudes across large-scale brain networks, that may play a pivotal role in promoting epileptogenicity. Our results further showed an increased presence of IEDs during NREM directly correlated with increased coupling between δ phase and β-γ amplitudes across large-scale brain networks.

Altogether, these results highlight the critical role of sleep instability in shaping epileptic activity, reinforcing N2 as the sleep stage most vulnerable to seizure generation, and suggest the presence of two possible types of δ-oscillations differently involved in the orchestration of physiological and pathological oscillations.

Analysis of local oscillations and large-scale synchrony reveal frequency-specific, EZ-specific differences between N2 and N3

In addition to the established δ-instability metric, two amplitude and two synchrony metrics were used to characterize spectral differences in local and network features between the EZ and nEZ, as well as between N2 and N3 sleep. The EZ and nEZ showed weak to moderate but distinct frequency-specific differences across sleep stages. During N3, the nEZ exhibited moderately stronger δ amplitude, reflecting the prominent slow-wave oscillations characteristic of N3. In contrast, during N2—when seizures most frequently occur in Sleep Hypermotor Epilepsy[20]—the EZ displayed stronger β-γ bistability, indicative of heightened epileptogenicity, consistent with focal epilepsy during resting-state[22]. However, synchrony differences between N2 and N3 were minimal in both the EZ and nEZ. Only during N3 did the EZ show moderate differences in the clustering coefficient for the δ phase, suggesting that its connected neighbors (both EZ and nEZ) are tightly connected. This also indicates that the elevated δ-band oscillations in the nEZ are coupled across regions.

Strong differences between the EZ and nEZ

The EZ exhibited stronger δ-band amplitudes, particularly during N2, coinciding with pathological δ-instability[19]. Rather than amplitudes, stronger bistability of the high-frequency oscillations in both N2 and N3 demarcating the EZ with large effect sizes, suggesting a pathological role[49] similar to that observed in focal epilepsy in resting-state[22]. Bistability showed a noticeable shift from 10–300 Hz in N2 to 4–150 Hz in N3. This slowing could be associated with decreased seizure risk in N3, similar to post-seizure slowing[50,51], which warrants further investigation.

On a large scale, the EZ exhibited stronger phase synchrony, including δ-band EVC and CC, indicating that the EZ and its neighbors (*i.e.*, both EZ and nEZ) are strongly connected. In contrast, only stronger β-γ EVC characterized the EZ, coinciding with concurrent strong β-γ bistability within the EZ, suggesting that these pathological features in fast oscillations are confined to the EZ and not its network neighbors. The strong δ-band EVC and CC, together with strong β-γ bistability and EVC, characterize

the EZ, implying a cross-frequency link between the slow δ phase and faster β-γ bistability.

CCA reveals strong correlations between δ phase and β–γ bistability

The PAC analysis revealed moderate differences between N2 and N3. We found stronger 1 Hz PAC connectivity between nEZ during N3, indicative of a strong modulatory effect of large-scale slow oscillations on faster brain rhythms[9]. On the other hand, 2–4 Hz slow waves of the nEZ strongly modulate the faster rhythms of the EZ, predominantly during N2. The latter could be linked to an epileptogenic mechanism if regions with strong δ phase coupled β–γ amplitudes also exhibited strong bistability in the β-γ band. These results implied the presence of at least two distinct δ oscillations, as previously reported in humans[52–54] and rodent studies[55].

In both N2 and N3, inward-PAC was correlated with bistability, with δ phase coupled β-γ amplitudes and β-γ band bistability as the strongest contributors, indicating that contacts with strongly δ phase coupled β-γ amplitudes also exhibited high β-γ bistability. Meanwhile, outward-PAC was correlated with phase synchrony, with θ and β-γ band outward PAC and δ-phase synchrony being the primary contributors, suggesting that contacts with strong δ-band phase synchrony also showed δ-phase coupling with θ and β-γ band amplitudes.

Altogether, these results suggest a link between heightened δ-phase synchrony and increased β-γ bistability mediated by cross-frequency coupling promoted during the most unstable substage of NREM. This supports the idea that increased instability of δ oscillations favors aberrant phase synchronization patterns that, via a cross-frequency coupling, in turn entrain a pathological network mechanism that supports the onset and spread of fast-activity bursts, particularly within the EZ.

Our findings align with and expand upon previous studies[15,56], reinforcing the concept that slow-wave instability is an inherent and fundamental feature of sleep. In people with epilepsy, this instability may be hijacked by epileptic activity, playing a crucial role in favoring the emergence of pathological dynamics[15,57]. Recent studies have further

refined this perspective, showing that arousal fluctuations, regulated by noradrenergic activity, are essential for maintaining sleep continuity, sleep-related memory processes, and cerebrospinal fluid dynamics[58]. These insights, combined with advances in animal models[59,60], offer new perspectives on the neurophysiological mechanisms underlying these dynamics, suggesting that altered arousal fluctuations may contribute to heightened cortical excitability, ultimately promoting sleep fragmentation and facilitating epileptic activity. This growing body of evidence may open new perspectives for therapeutic strategies. Beyond conventional antiseizure medications, modulating sleep physiology may represent a promising complementary approach. Pharmacological or neuromodulatory interventions targeting arousal fluctuations could help stabilize sleep, potentially mitigating epilepsy-related sleep disturbances and reducing seizure burden. Future research should explore whether optimizing sleep stability—through targeted drugs or closed-loop neuromodulation—can disrupt this pathological cycle, offering novel treatment avenues for sleep-related epilepsies.

Scope and limitations

This study included fourteen subjects due to strict selection criteria and practical challenges, reducing the number of subjects suitable for analysis. However, the small sample size was offset by strong statistical power, supported by a relatively large dataset of 190 epochs, totaling 32 hours of interictal sleep SEEG data with uninterrupted N2 and N3 recordings. Patients with well-delineated FCD type II foci, who predominantly have seizures during sleep, served as an ideal disease model for testing our hypothesis. Further investigation is needed to explore how PAC interconnects δ phase and β-γ bistability and to determine whether our findings generalize to other seizure types or patients with more complex EZ networks.

Acknowledgements

This project is supported by: NEXTGENERATIONEU (NGEU), the Ministry of University and Research, and National Recovery and Resilience Plan project MNESYS (PE0000006; A Multiscale Integrated Approach to the Study of the Nervous

System in Health and Disease; DN. 1553 11.10.2022) awarded to L.N. and G.A. A Sigrid Jusélius Foundation fellowship (210527) awarded to SHW.

Author Contributions

Conception and design of the study: GA, LN, JMP, & SHW. Data acquisition and analysis: GB, FZ, LN, & GA. Drafting a significant portion of the manuscript or figures: GA, GB, LN, & SHW. All authors edited and approved the final draft.

Conflicts of Interest

All authors have no conflict of interest to declare.

Data availability

Raw data and patient information cannot be shared due to Italian governing laws and Ethical Committee restrictions. Interim results, as well as final processed data that support the findings of this study, are available from the corresponding authors upon reasonable request.

References

1. Minecan D, Natarajan A, Marzec M, Malow B. Relationship of Epileptic Seizures to Sleep Stage and Sleep Depth. Sleep 2002;25(8):56–61.

2. Frauscher B, von Ellenrieder N, Dubeau F, Gotman J. EEG desynchronization during phasic REM sleep suppresses interictal epileptic activity in humans. Epilepsia 2016;57(6):879–888.

3. Nobili L, Frauscher B, Eriksson S, et al. Sleep and epilepsy: A snapshot of knowledge and future research lines. J. Sleep Res. 2022;31(4):e13622.

4. Steriade M, Amzica F, Contreras D. Cortical and thalamic cellular correlates of electroencephalographic burst-suppression. Electroencephalogr. Clin. Neurophysiol. 1994;90(1):1–16.

5. Steriade M, Contreras D, Amzica F. Synchronized sleep oscillations and their paroxysmal developments. Trends Neurosci. 1994;17(5):199–208.

6. Beenhakker MP, Huguenard JR. Neurons that fire together also conspire together: is normal sleep circuitry hijacked to generate epilepsy? Neuron 2009;62(5):612–632.

7. Gibbs SA, Proserpio P, Francione S, et al. Clinical features of sleep-related hypermotor epilepsy in relation to the seizure-onset zone: A review of 135 surgically treated cases. Epilepsia 2019;60(4):707–717.

8. Bernard C, Frauscher B, Gelinas J, Timofeev I. Sleep, oscillations, and epilepsy. Epilepsia 2023;64 Suppl 3(Suppl 3):S3–S12.

9. Steriade M. Grouping of brain rhythms in corticothalamic systems. Neuroscience 2006;137(4):1087–1106.

10. Mölle M, Yeshenko O, Marshall L, et al. Hippocampal Sharp Wave-Ripples Linked to Slow Oscillations in Rat Slow-Wave Sleep. J. Neurophysiol. 2006;96(1):62–70.

11. Staresina BP, Bergmann TO, Bonnefond M, et al. Hierarchical nesting of slow oscillations, spindles and ripples in the human hippocampus during sleep. Nat. Neurosci. 2015;18(11):1679–1686.

12. Klinzing JG, Mölle M, Weber F, et al. Spindle activity phase-locked to sleep slow oscillations. NeuroImage 2016;134:607–616.

13. Oyanedel CN, Durán E, Niethard N, et al. Temporal associations between sleep slow oscillations, spindles and ripples. Eur. J. Neurosci. 2020;52(12):4762–4778.

14. Frauscher B, von Ellenrieder N, Ferrari-Marinho T, et al. Facilitation of epileptic activity during sleep is mediated by high amplitude slow waves. Brain J. Neurol. 2015;138(Pt 6):1629–1641.

15. Parrino L, Smerieri A, Spaggiari MC, Terzano MG. Cyclic alternating pattern (CAP) and epilepsy during sleep: how a physiological rhythm modulates a pathological event. Clin. Neurophysiol. 2000;111:S39–S46.

16. Herman ST, Walczak TS, Bazil CW. Distribution of partial seizures during the sleep--wake cycle: differences by seizure onset site. Neurology 2001;56(11):1453–1459.

17. Vanhatalo S, Palva JM, Holmes MD, et al. Infraslow oscillations modulate excitability and interictal epileptic activity in the human cortex during sleep. Proc. Natl. Acad. Sci. U. S. A. 2004;101(14):5053–5057.

18. Parrino L, Halasz P, Tassinari CA, Terzano MG. CAP, epilepsy and motor events during sleep: the unifying role of arousal. Sleep Med. Rev. 2006;10(4):267–285.

19. Zubler F, Rubino A, Lo Russo G, et al. Correlating Interictal Spikes with Sigma and Delta Dynamics during Non-Rapid-Eye-Movement-Sleep [Internet]. Front. Neurol. 2017;8[cited 2025 Jan 29] Available from: https://www.frontiersin.org/journals/neurology/articles/10.3389/fneur.2017.00288/full

20. Proserpio P, Loddo G, Zubler F, et al. Polysomnographic features differentiating disorder of arousals from sleep-related hypermotor epilepsy. Sleep 2019;42(12):zsz166.

21. Wang SH, Siebenhühner F, Arnulfo G, et al. Critical-like Brain Dynamics in a Continuum from Second- to First-Order Phase Transition. J. Neurosci. 2023;43(45):7642–7656.

22. Wang SH, Arnulfo G, Nobili L, et al. Neuronal synchrony and critical bistability: Mechanistic biomarkers for localizing the epileptogenic network. Epilepsia 2024;65(7):2041–2053.

23. Thom R. Structural Stability And Morphogenesis. Boca Raton: CRC Press; 2018.

24. Villa Martín P, Bonachela JA, Levin SA, Muñoz MA. Eluding catastrophic shifts. Proc. Natl. Acad. Sci. U. S. A. 2015;112(15):E1828-36.

25. Schwoon N, Khazali MF, Brandt A, et al. Sleep increases broadband fast oscillations in the epileptic focus of patients with focal cortical dysplasia [Internet]. 2025;2025.02.18.25322331.[cited 2025 Mar 4] Available from: https://www.medrxiv.org/content/10.1101/2025.02.18.25322331v1

26. Monto S, Vanhatalo S, Holmes MD, Palva JM. Epileptogenic Neocortical Networks Are Revealed by Abnormal Temporal Dynamics in Seizure-Free Subdural EEG. Cereb. Cortex 2007;17(6):1386–1393.

27. Johnson GW, Doss DJ, Morgan VL, et al. The Interictal Suppression Hypothesis in focal epilepsy: network-level supporting evidence. Brain J. Neurol. 2023;146(7):2828–2845.

28. Fuscà M, Siebenhühner F, Wang SH, et al. Brain criticality predicts individual levels of inter-areal synchronization in human electrophysiological data. Nat. Commun. 2023;14(1):4736.

29. Wang SH, Marzulli M, Arnulfo G, et al. Machine Learning Models Trained in a Low-Dimensional Latent Space for Epileptogenic Zone (EZ) Localization [Internet]. In: 2024 32nd European Signal Processing Conference (EUSIPCO). 2024 p. 1586–1590.[cited 2025 Mar 4] Available from: https://ieeexplore.ieee.org/abstract/document/10715112

30. Arnulfo G, Wang SH, Myrov V, et al. Long-range phase synchronization of high-frequency oscillations in human cortex. Nat. Commun. 2020;11(1):5363.

31. Siebenhühner F, Wang SH, Arnulfo G, et al. Genuine cross-frequency coupling networks in human resting-state electrophysiological recordings. PLOS Biol. 2020;18(5):e3000685.

32. Cocchi L, Gollo LL, Zalesky A, Breakspear M. Criticality in the brain: A synthesis of neurobiology, models and cognition. Prog. Neurobiol. 2017;158:132–152.

33. Beggs JM. The criticality hypothesis: how local cortical networks might optimize information processing. Philos. Trans. R. Soc. Math. Phys. Eng. Sci. 2007;366(1864):329–343.

34. Beggs JM. Addressing skepticism of the critical brain hypothesis [Internet]. Front. Comput. Neurosci. 2022;16[cited 2025 Mar 17] Available from: https://www.frontiersin.org/journals/computational-neuroscience/articles/10.3389/fncom.2022.703865/full

35. Nobili L, Cardinale F, Magliola U, et al. Taylor's focal cortical dysplasia increases the risk of sleep-related epilepsy. Epilepsia 2009;50(12):2599–2604.

36. Rosenow F, Lüders H. Presurgical evaluation of epilepsy. Brain J. Neurol. 2001;124(Pt 9):1683–1700.

37. Engel J. Update on surgical treatment of the epilepsies. Neurology 1993;43(8):1612–1612.

38. Lüders HO, Najm I, Nair D, et al. The epileptogenic zone: general principles. Epileptic Disord. Int. Epilepsy J. Videotape 2006;8 Suppl 2:S1-9.

39. von Ellenrieder N, Peter-Derex L, Gotman J, Frauscher B. SleepSEEG: automatic sleep scoring using intracranial EEG recordings only. J. Neural Eng. 2022;19(2):026057.

40. Tallon-Baudry C, Bertrand O, Delpuech C, Pernier J. Stimulus Specificity of Phase-Locked and Non-Phase-Locked 40 Hz Visual Responses in Human. J. Neurosci. 1996;16(13):4240–4249.

41. Freyer F, Roberts JA, Ritter P, Breakspear M. A Canonical Model of Multistability and Scale-Invariance in Biological Systems. PLOS Comput. Biol. 2012;8(8):e1002634.

42. Palva JM, Wang SH, Palva S, et al. Ghost interactions in MEG/EEG source space: A note of caution on inter-areal coupling measures. NeuroImage 2018;173:632–643.

43. Siebenhühner F, Wang SH, Palva JM, Palva S. Cross-frequency synchronization connects networks of fast and slow oscillations during visual working memory maintenance. eLife 2016;5:e13451.

44. Hotelling H. Relations Between Two Sets of Variates. Biometrika 1936;28(3/4):321–377.

45. Smith SM, Nichols TE, Vidaurre D, et al. A positive-negative mode of population covariation links brain connectivity, demographics and behavior. Nat. Neurosci. 2015;18(11):1565–1567.

46. Pedregosa F, Varoquaux G, Gramfort A, et al. Scikit-learn: Machine Learning in Python. J. Mach. Learn. Res. 2011;12(85):2825–2830.

47. Benjamini Y, Hochberg Y. Controlling the False Discovery Rate: A Practical and Powerful Approach to Multiple Testing. J. R. Stat. Soc. Ser. B Methodol. 1995;57(1):289–300.

48. von Ellenrieder N, Gotman J, Zelmann R, et al. How the Human Brain Sleeps: Direct Cortical Recordings of Normal Brain Activity. Ann. Neurol. 2020;87(2):289–301.

49. Frauscher B, Bartolomei F, Kobayashi K, et al. High-frequency oscillations: The state of clinical research. Epilepsia 2017;58(8):1316–1329.

50. Kramer MA, Truccolo W, Eden UT, et al. Human seizures self-terminate across spatial scales via a critical transition. Proc. Natl. Acad. Sci. 2012;109(51):21116–21121.

51. Jirsa VK, Stacey WC, Quilichini PP, et al. On the nature of seizure dynamics. Brain J. Neurol. 2014;137(Pt 8):2210–2230.

52. Amzica F, Steriade M. Electrophysiological correlates of sleep delta waves1. Electroencephalogr. Clin. Neurophysiol. 1998;107(2):69–83.

53. Crunelli V, Hughes SW. The slow (<1 Hz) rhythm of non-REM sleep: a dialogue between three cardinal oscillators. Nat. Neurosci. 2009;13(1):9.

54. Bernardi G, Betta M, Ricciardi E, et al. Regional Delta Waves In Human Rapid Eye Movement Sleep. J. Neurosci. 2019;39(14):2686.

55. Hubbard J, Gent TC, Hoekstra MMB, et al. Rapid fast-delta decay following prolonged wakefulness marks a phase of wake-inertia in NREM sleep. Nat. Commun. 2020;11(1):3130.

56. Terzano MG, Parrino L, Anelli S, et al. Effects of generalized interictal EEG discharges on sleep stability: assessment by means of cyclic alternating pattern. Epilepsia 1992;33(2):317–326.

57. Manni R, Zambrelli E, Bellazzi R, Terzaghi M. The relationship between focal seizures and sleep: an analysis of the cyclic alternating pattern. Epilepsy Res. 2005;67(1–2):73–80.

58. Lüthi A, Nedergaard M. Anything but small: Microarousals stand at the crossroad between noradrenaline signaling and key sleep functions. Neuron 2025;113(4):509–523.

59. Cardis R, Lecci S, Fernandez LM, et al. Cortico-autonomic local arousals and heightened somatosensory arousability during NREMS of mice in neuropathic pain. eLife 2021;10:e65835.

60. Osorio-Forero A, Cardis R, Vantomme G, et al. Noradrenergic circuit control of non-REM sleep substates. Curr. Biol. 2021;31(22):5009-5023.e7.

Figures

Fig 1.

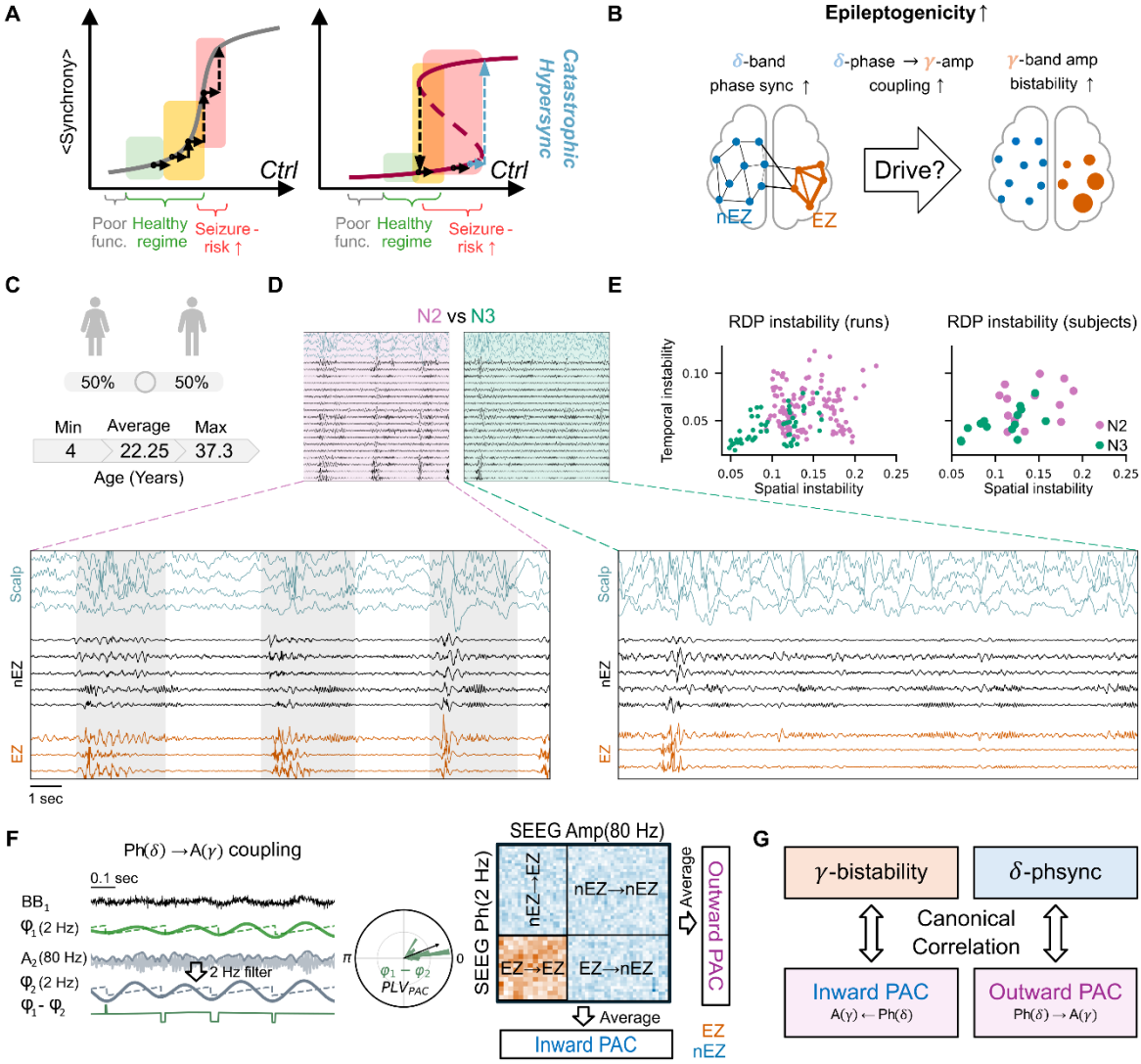

Study schematics. **(A)** As excitability (ctrl) increases, the nEZ exhibits classic criticality with unimodal mean synchrony (left), whereas the EZ displays strong bistability (right). **(B)** The EZ shows strong δ-band synchrony (left) and β-γ band bistability (right). *Hypothesis*: a mechanistic link between δ phase and β-γ bistability (center). **(C)** Subjects. **(D)** Exemplary bipolar referenced traces. Only a subset of nEZ channels is shown. **(E)** Epoch-level (left) and individual-level (right) spatial and temporal δ-instability during N2 (pink) and N3 (green). **(F)** Left: PAC assessment. Right: in a PAC connectivity matrix (*e.g.*, 2→80 Hz), averaging a row represents *outward connectivity*, characterizing how one contact's 2 Hz phase couples with the 80 Hz amplitudes of the network. Conversely, averaging a column represents *inward PAC*, characterizing how one contact's 80 Hz amplitude is coupled with the 2 Hz phase of the network. **(G)** Canonical correlation analysis (CCA) is employed to address whether the δ phase is coupled with β–γ bistability through PAC.

Fig 2.

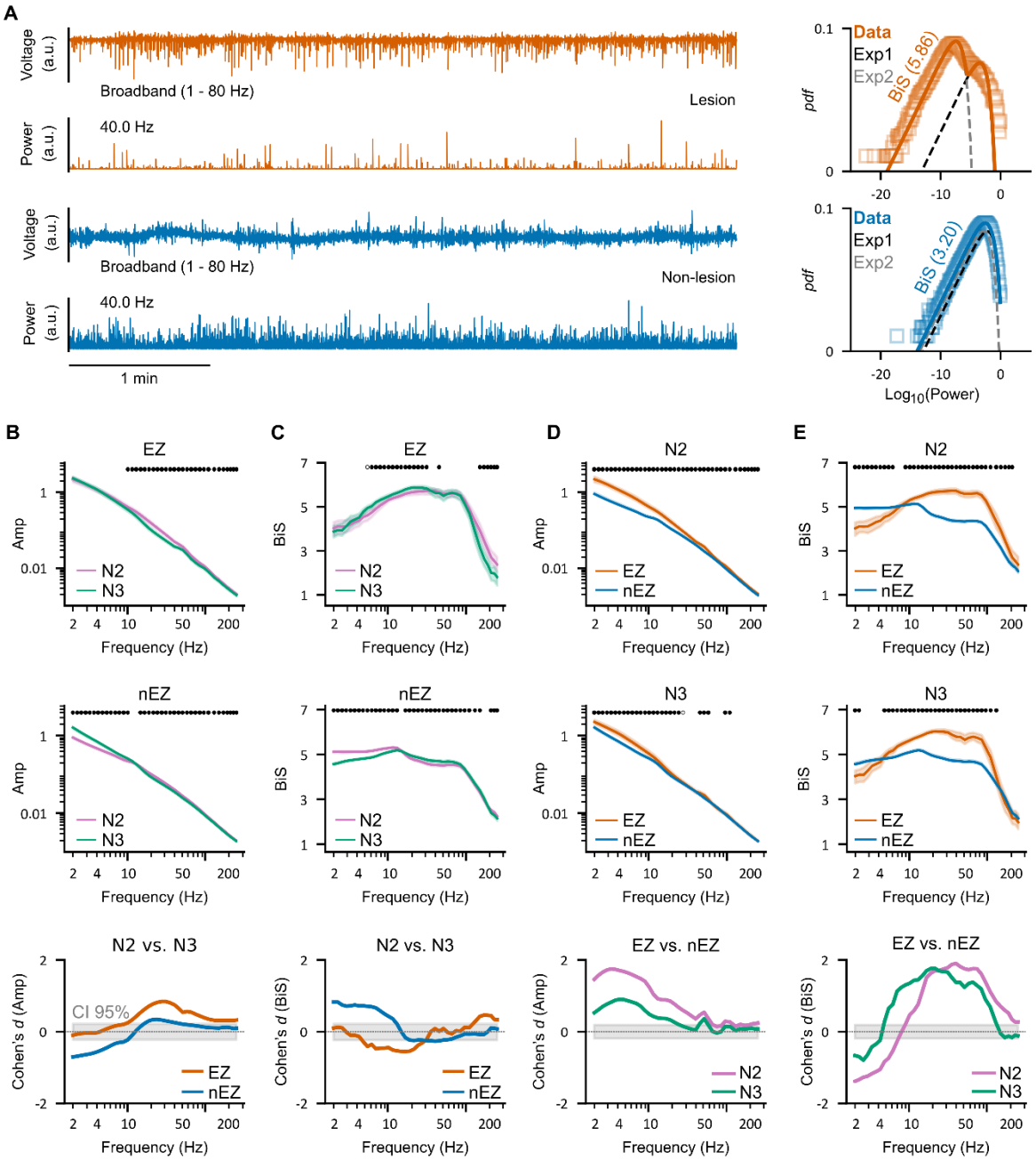

The EZ exhibits stronger local β–γ bistability in both N2 and N3. **(A)** Left: bipolar-referenced broad-band and its 40 Hz narrow-band power time series from an EZ contact (orange) and a nearby nEZ (blue) contact from a N2 epoch. Right: fitting for the bistability index (BiS). **(B)** Mean narrow-band amplitude spectrum of N2 and N3 epochs for EZ (top), nEZ (middle), and effect size of the difference between N2 and N3 (bottom). **(C)** The same as in **(B)** for bistability. **(D)** Mean narrow-band amplitude spectrum of EZ and nEZ during N2 (top), N3 (middle), and effect size of the difference between EZ and nEZ (bottom). **(E)** The same as in **(D)** for bistability. Sample size in **(B–E)**: (N_{EZ}=93; N_{nEZ}=1046 contacts); on top of **(B–E),** markers indicate difference (Wilcoxon rank-sum test, $p < 0.05$, corrected with Benjamini-Hochberg procedure); shaded areas indicate 2.5% and 97.5%-tile of 10,000 surrogates. Effect sizes of Cohen's *d*: small 0.2), medium (0.5), and large (≥0.8).

Fig 3.

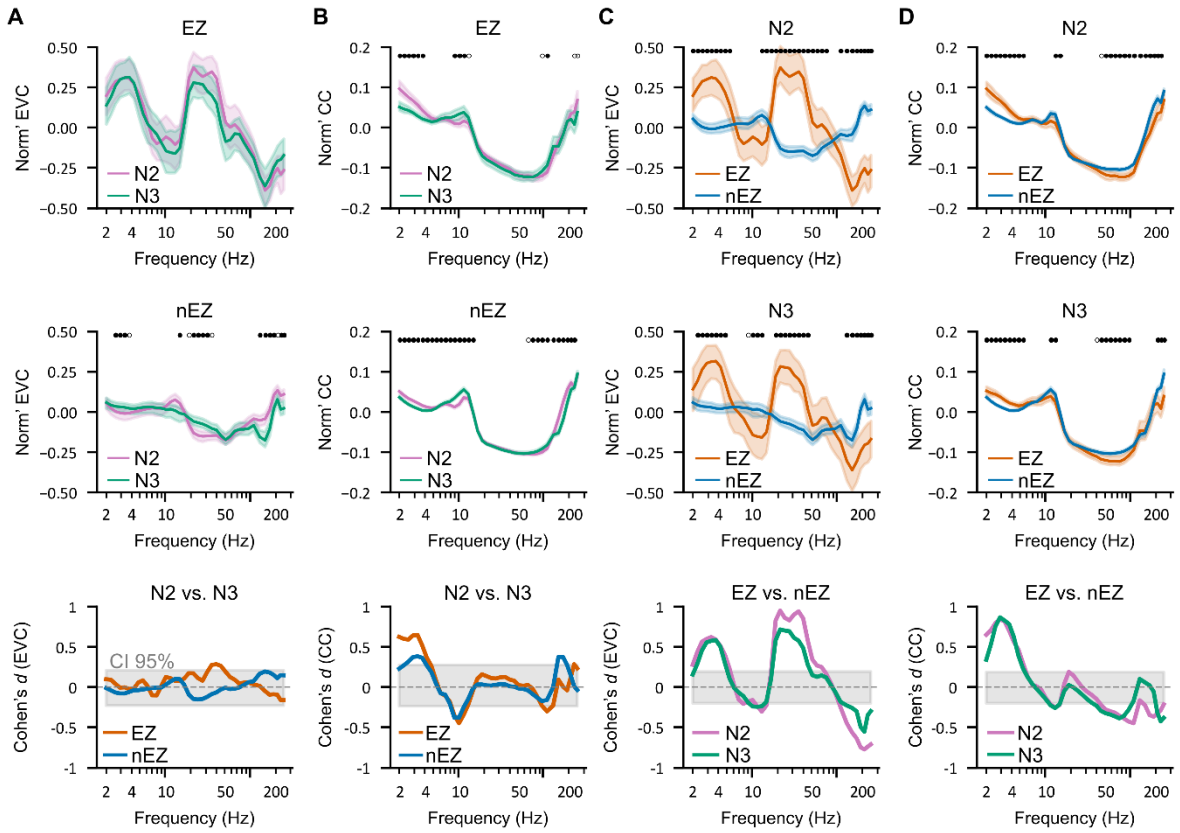

The EZ exhibits stronger large-scale synchrony than the nEZ in both N2 and N3. **(A)** Normalized eigenvector centrality (EVC) during N2 and N3 for the EZ (top), nEZ (middle), and the effect size of the differences between N2 and N3 (bottom). **(B)** The same as in **(A)** for clustering coefficient (CC). **(C)** Normalized EVC of EZ and nEZ during N2 (top) and N3 (middle), and the effect size of the differences between EZ and nEZ during N2 and N3 (bottom). **(D)** The same as in **(C)** for CC. Sample size in **(A–D)**: (N_{EZ}=93; N_{nEZ}=1046 contacts); markers in **(A–D)** indicate difference (Wilcoxon rank-sum test, $p < 0.05$, FDR corrected with Benjamini-Hochberg procedure); shaded areas in top and middle row panels represent the variability computed from 100 bootstraps (95th percentile), shaded areas in bottom row panels indicate 2.5% and 97.5%-tile of 10'000 surrogates. Cohen classified effect sizes as small (d = 0.2), medium (d = 0.5), and large ($d \geq 0.8$).

Fig 4.

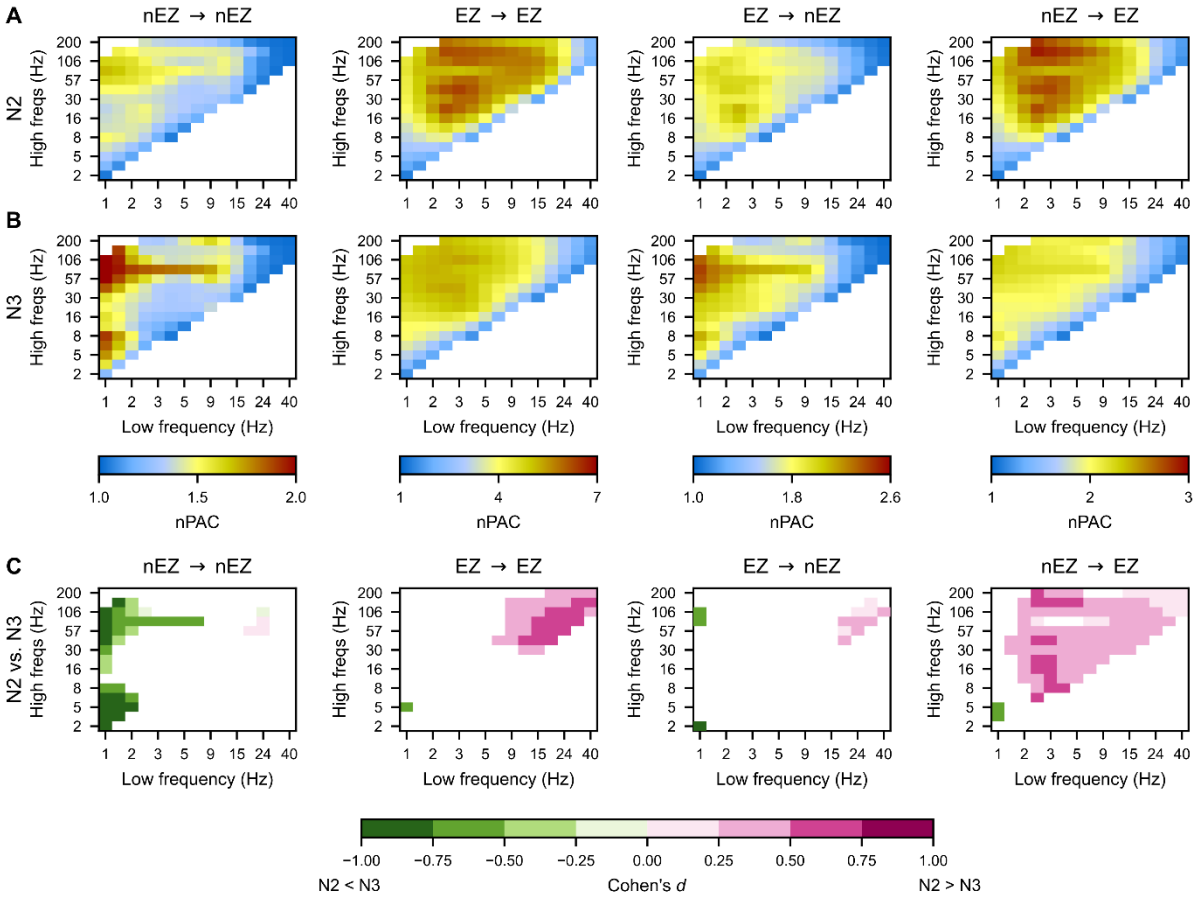

PAC between the 2–5 Hz phase in the nEZ and fast amplitudes in the EZ is stronger during N2 than N3. **(A–B)** Cohort average of normalized PAC (nPAC) for **(A)** N2 and **(B)** N3; nPAC = $PLV_{PAC,observed}/PLV_{PAC,surrogate}$ ($N_{surrogate}$ = 100) so that nPAC > 1 indicates PAC above the null hypothesis level. **(C)** Effect size of the difference between N2 and N3 sleep stages. Only effect sizes for which the differences between N2 and N3 were statistically significant (p < 0.05, corrected with Benjamini-Hochberg procedure) are presented.

Fig 5.

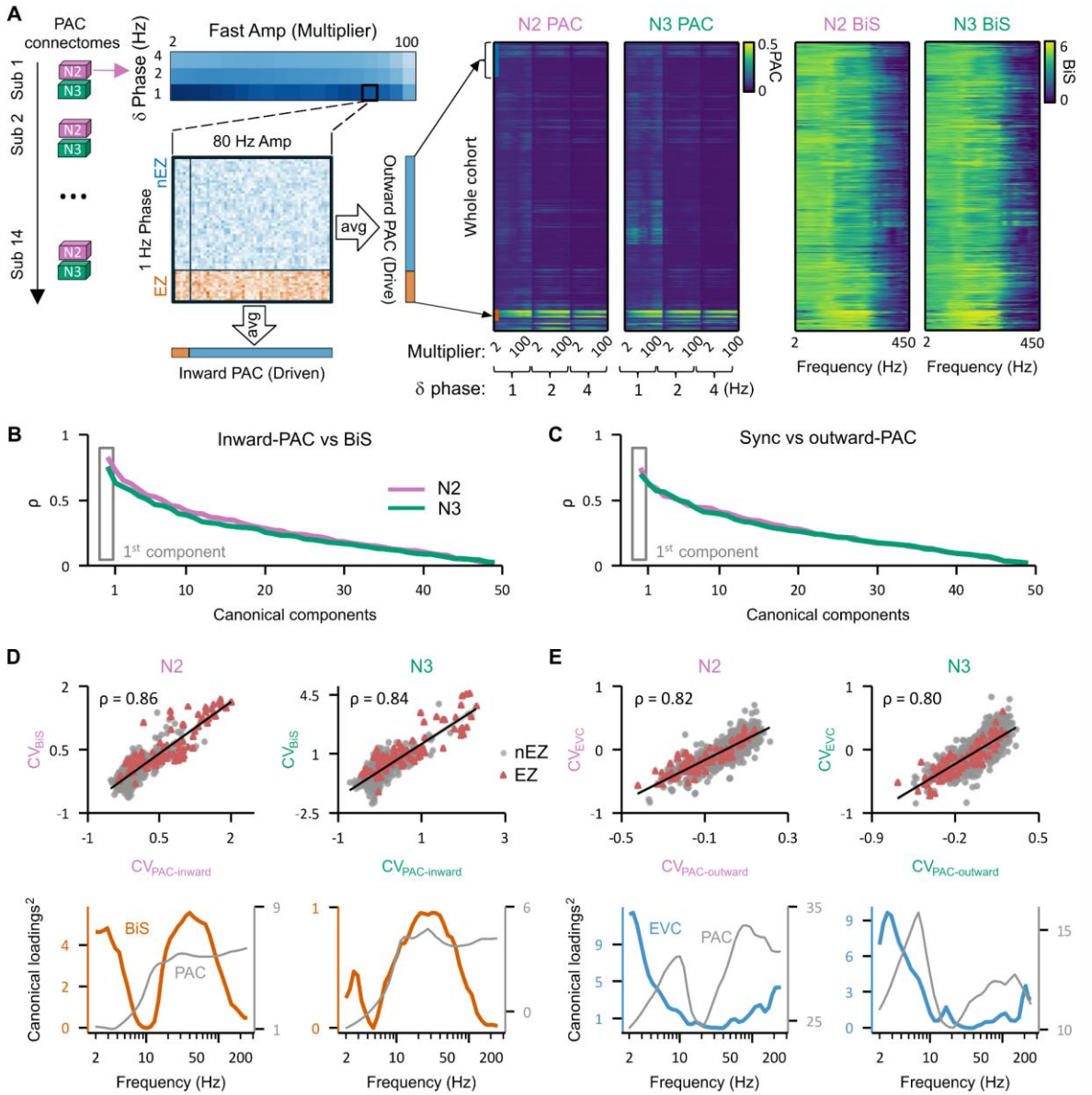

CCA reveals a link between inward-PAC and bistability as well as between outward-PAC and synchrony. **(A)** Illustration of the preparation of the feature data for CCA. **(B–C)** Pearson's correlations (ρ) between canonical variates (CV) of **(B)** inward-PAC and bistability, **(C)** outward-PAC and synchrony (Sample: N_{EZ}=93; N_{nEZ}=1046 contacts pooled from 14 subjects). EVC: eigenvector centrality. **(D)** Top: the corresponding canonical covariates for the 1st component highlighted in **(B)**. Bottom: squared loadings for the covariates, an indicator of the contribution of each frequency to the observed canonical correlation. The gray PAC curve is the average loading across [1, 2, 4] Hz PAC. **(E)** The same as **(D)** for **(C)**.

Tables

Table 1

Established biomarkers			Novel biomarkers: Interictal resting-state SEEG								
	N2	N3		δ	θ	α	σ	β	γ_1	γ_2	γ_3
δ-instability	☑		LRTCs	☑	☑						
δ-oscillations		☑	Bistability ↑					☑	☑	☑	
K-complexes	☑		Inhibition					☑	☑	☑	
IEDs	☑		1:1 PLV	☑	☑	☑					
Seizures	☑		n:m PAC	EZ–EZ: Θ(δ–α) → A(σ–γ_3) ↑							

Established and novel biomarkers proposed in prior arts. IEDs: interictal epileptiform discharges; PLV: phase-locking value; LRTCs: power-law scaling in long-range temporal correlations; PAC: cross-frequency phase-amplitude coupling. EZ: epileptogenic zone. Canonical bands: δ (1–4 Hz), θ (4–8 Hz), α (8–12 Hz), σ (12–16 Hz), β (16–30 Hz), γ_1 (30–60 Hz), γ_2 (60–80 Hz), γ_3 (80–250 Hz), γ → $\gamma_{1\text{-}3}$.

Table 2

Subject	01	02	03	04	05	06	07	08	09	10	11	12	13	14	Tot.
N2 epochs	7	8	14	10	21	4	8	7	8	11	8	4	12	12	134
N3 epochs	5	7	8	3	2	2	2	3	7	5	4	2	4	2	56
EZ channels	14	2	9	7	11	7	3	4	6	9	3	4	8	6	93
nEZ channels	53	67	66	88	55	73	76	116	115	69	74	98	53	43	1046

Dataset description. Individual number of recorded epochs for N2 and N3, number of channels recording from EZ and nEZ, and cumulative total elements.